Sustainable Energy & Fuels

ROYAL SOCIETY OF CHEMISTRY

PAPER

View Article Online
View Journal | View Issue

Check for updates

Cite this: *Sustainable Energy Fuels*, 2022, **6**, 143

Electrocatalytic reduction of protons to dihydrogen by the cobalt tetraazamacrocyclic complex $[Co(N_4H)Cl_2]^+$: mechanism and benchmarking of performances†‡

Cheng-Bo Li,§[ab] Andrew J. Bagnall,§[bc] Dongyue Sun,[b] Julia Rendon,[bd] Matthieu Koepf,[b] Serge Gambarelli,[d] Jean-Marie Mouesca,[d] Murielle Chavarot-Kerlidou[b] and Vincent Artero *[b]

The cobalt tetraazamacrocyclic $[Co(N_4H)Cl_2]^+$ complex is becoming a popular and versatile catalyst for the electrocatalytic evolution of hydrogen, because of its stability and superior activity in aqueous conditions. We present here a benchmarking of its performances based on the thorough analysis of cyclic voltammograms recorded under various catalytic regimes in non-aqueous conditions allowing control of the proton concentration. This allowed a detailed mechanism to be proposed with quantitative determination of the rate-constants for the various protonation steps, as well as identification of the amine function of the tetraazamacrocyclic ligand to act as a proton relay during H_2 evolution.

Received 19th August 2021
Accepted 4th November 2021

DOI: 10.1039/d1se01267c

rsc.li/sustainable-energy

Molecular cobalt complexes are popular and versatile catalysts for the electrocatalytic evolution of hydrogen.[1–5] Recently, the cobalt complex $[Co(N_4H)Cl_2]^+$ (**Cat1**, Fig. 1) based on the tetraazamacrocyclic 2,12-dimethyl-3,7,11,17-tetraazabicyclo[11.3.1]heptadeca-1(17),2,11,13,15-pentaene ligand,[6] described by Karn and Busch in 1966, has received increased interest[7–9] namely because this catalyst proves active and stable for the evolution of H_2 from fully aqueous solutions.[7–17] A study carried out under homogeneous conditions using chemical reductants or photochemical activation confirmed the superior activity of **Cat1** in fully aqueous media,[18] and X-ray absorption spectroscopic monitoring of a homogeneous photocatalytic system for H_2 evolution based on **Cat1** indicated an ECEC mechanism (E = monoelectronic electrochemical reduction, C = protonation step) starting from the bisaqua Co(II) complex.[13,14] However, very few metrics are currently available to benchmark the catalytic activity of this compound. **Cat1** was included in a benchmarking study for H_2-evolving electrocatalysts carried out in aqueous electrolyte[19] but under quite acidic conditions likely to induce reductive degradation of the ligand during the test and formation of metallic particles responsible for the observed HER activity.[20,21] To gain quantitative information on the H_2 evolution mechanism mediated by **Cat1**, we therefore revisited the non-aqueous conditions investigated by Lau and coworkers,[22] where it is easier to control the concentration and chemical potential of protons.[23]

The cyclic voltammogram of **Cat1** (perchlorate salt) in CH_3CN (with 0.1 M $^nBu_4NBF_4$, Fig. 2 and S1‡) displays two quasi-reversible systems at −0.47 V (ΔE_p = 92 mV) and −0.96 V (ΔE_p = 86 mV) *vs.* Fc^+/Fc, corresponding to the $Co^{III/II}$ and $Co^{II/I}$ redox processes, respectively, based on previous literature. Of note, we will formally use the Co^I notation throughout this article, while the electronic state could also correspond to a reduced N_4H ligand (π-radical anion) antiferromagnetically

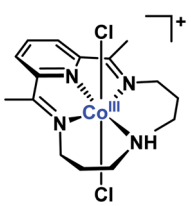

$[Co(N_4H)Cl_2]^+$ (**Cat1**)

Fig. 1 Structure of **Cat1**.

[a]*Key Laboratory of Synthetic and Natural Functional Molecule of the Ministry of Education, The Energy and Catalysis Hub, College of Chemistry and Materials Science, Northwest University, Xi'an 710127, China*

[b]*Univ. Grenoble Alpes, CNRS, CEA, IRIG, Laboratoire de Chimie et Biologie des Métaux, 17 Rue des Martyrs, F-38054 Grenoble, Cedex, France. E-mail: vincent.artero@cea.fr*

[c]*Ångström Laboratory, Department of Chemistry, Uppsala University, SE75120 Uppsala, Sweden*

[d]*Univ. Grenoble Alpes, CNRS, CEA/IRIG-SyMMES, 17 Rue des Martyrs, F-38054 Grenoble, Cedex, France*

† In memory of Dr Jean-Michel Savéant.

‡ Electronic supplementary information (ESI) available. See DOI: 10.1039/d1se01267c

§ Equal contribution.

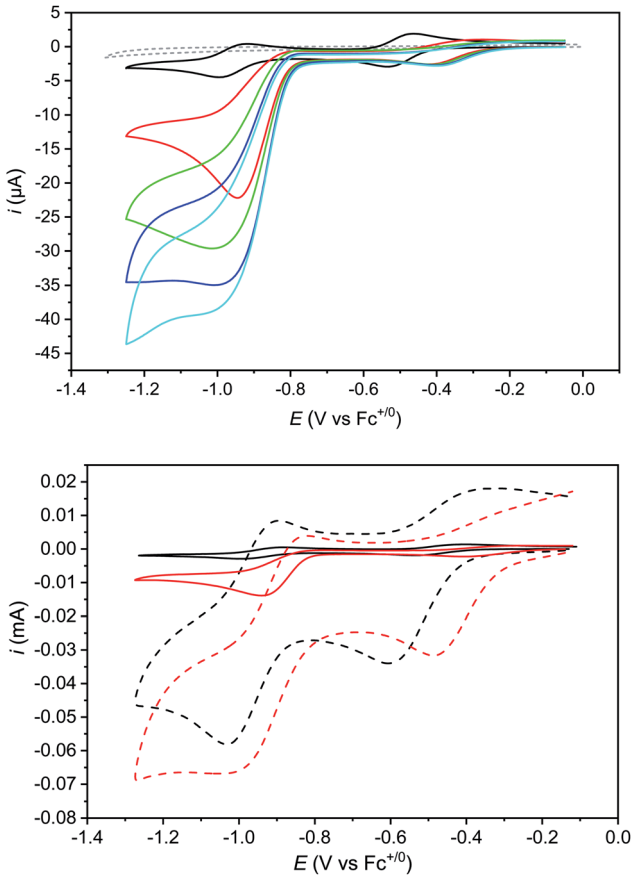

Fig. 2 Top: cyclic voltammograms of **Cat1** (0.5 mM) in CH_3CN (+0.1 M $^nBu_4NBF_4$) recorded at a glassy carbon electrode (1.6 mm diameter) in the absence (black trace) and in the presence of 5.0 (red trace), 10.0 (green trace), 12.5 (navy trace) and 15.0 mM (cyan trace) *p*-cyanoanilinium tetrafluoroborate; scan rate: 100 mV s^{-1}. A control voltammogram of 15 mM *p*-cyanoanilinium tetrafluoroborate without **Cat1** (gray dashed trace) is shown for comparison; bottom: cyclic voltammograms of **Cat1** (0.5 mM) in CH_3CN (+0.1 M $^nBu_4NBF_4$) recorded at a glassy carbon electrode in the absence (black) and in the presence (red) of 5 mM *p*-cyanoanilinium tetrafluoroborate; scan rate: 0.1 (solid) and 10 V s^{-1} (dashed). See Fig. S5‡ for control voltammograms without catalyst under similar conditions.

coupled to a low-spin Co(II) ion.[24] A third ligand-centered process is observed at −1.89 V (ΔE_p = 69 mV) *vs.* Fc^+/Fc.[22] Upon addition of *p*-cyanoanilinium tetrafluoroborate (pK_a = 7.0 in CH_3CN)[25] acting as a proton source, a catalytic wave develops on the top of the $Co^{II/I}$ wave as previously described.[22] This electrocatalytic behavior corresponds to H_2 evolution with >90% faradaic yield[22] and nicely mirrors the one observed for **Cat1** in mildly acidic aqueous solution.[11,13,22] The addition of stronger acids such as $HBF_4 \cdot Et_2O$ or CF_3SO_3H also triggers H_2 evolution catalysis but is detrimental to the stability of **Cat1** at high concentration. **Cat1** is unable to catalyze the reduction of acids with higher pK_a values, starting with *p*-toluenesulfonic acid (pK_a = 8.3 in CH_3CN).[26]

Noteworthily, the addition of acid also affects the $Co^{III/II}$ system, which shifts to more positive potentials and partly loses reversibility. ^1H NMR experiments confirmed that the Co^{III} form of **Cat1** is not protonated under these conditions (Fig. S2‡), neither does *p*-cyanoaniline coordinate to any of the Co^{III}, Co^{II} and Co^{I} states of **Cat1** (Fig. S3‡) in the absence of acid. However, when 5 equivalents of *p*-cyanoanilinium tetrafluoroborate is added to an electrochemically-generated solution of the Co^{II} form of **Cat1**, the EPR signal is significantly changed, from a broad signal centered at $g_1 = 2.240$, $g_2 = 2.130$ and $g_3 = 2.004$ to a better resolved spectrum characteristic for a low spin d^7 ($S = \frac{1}{2}$) electronic configuration of Co (Fig. 3). It furthermore displays a 5-line superhyperfine structure with an intensity ratio of 1 : 2 : 3 : 2 : 1 and a coupling constant of 45 Hz in line with the coordination of two equivalent nitrogen-based ligands. Of note, a similar behavior was observed when the Co^{II} form of **Cat1** was prepared by chemical reduction with cobaltocene instead of exhaustive bulk electrolysis (Fig. S4‡). No such change is observed when *p*-cyanoaniline is added (Fig. S4‡). When $HBF_4 \cdot Et_2O$ is used as proton source instead of *p*-cyanoanilinium tetrafluoroborate, this superhyperfine structure is changed to a 3-line structure with a coupling constant of 40 Hz (Fig. 3), suggesting the coordination of a single nitrogen-based axial ligand, CH_3CN being the only plausible one under these conditions. In the former case, coordination of CH_3CN and *p*-cyanoanilinium (or *p*-cyanoaniline generated *in situ* upon protonation of the complex) can be considered without being possible to discriminate one from the other at the EPR level. Taken all together, these observations suggest (i) protonation of the ligand in **Cat1** occurs upon reduction from the Co^{III} to the Co^{II} state in the presence of acid; (ii) at the same time, chloride axial ligands are displaced for nitrogen ligands; (iii) the nature and number of axial ligands depend on the nature of the acid employed. It should also be underlined that the binding of one *vs.* two ligands in the cobalt + II oxidation state likely depends on a subtle balance of their donating ability, as previously stated

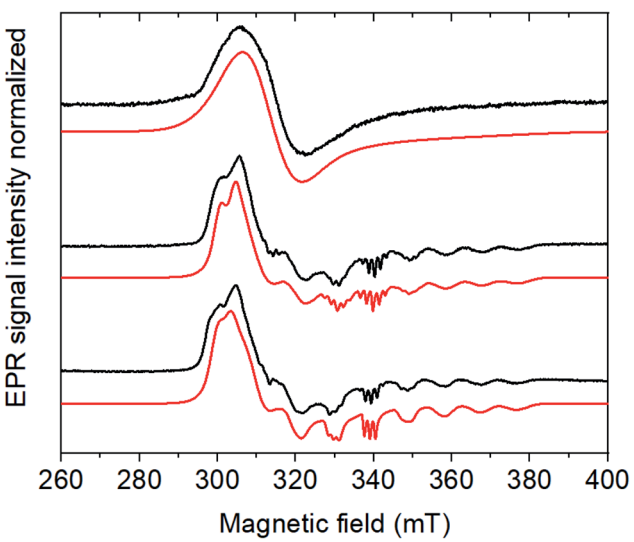

Fig. 3 CW X-band EPR spectra (9.65 GHz) of the electrochemically generated Co^{II} form of **Cat1** (0.5 mM) as prepared (top), with 5 eq. of the acids *p*-cyanoanilinium tetrafluoroborate (middle), HBF_4 (bottom) and their respective simulations in red. Experimental conditions: 30 K, 1 mW microwave power, 1600 G field sweep. Simulation parameters are reported in Table S1.‡

for **Cat1** (ref. 11) and also found for cobaloximes and related cobalt diimine–dioxime complexes.[27–30] A possible structure of **Co^{II}LH**, in line with a previous proposition,[13] is shown in Scheme 1.

Although the formation of the protonated Co^{II} derivative of **Cat1** falls into the proton-coupled electron transfer classification, the cathodic peak potential does not follow the increase of 29 mV per decade of acid concentration expected for an irreversible EC process with a fully displaced protonation equilibrium (*e.g.* in the pure kinetic KP zone);[31] rather the cathodic peak potential rapidly shifts to a new value upon addition of acid and then keeps this value unchanged upon further addition (Fig. 2). This behavior is characteristic of the extraordinary kinetic (KE) zone,[31] with fast protonation of the Co^{II} species so that, even with few equivalents of acid added, the new wave is observed at a potential close to the apparent standard potential of the **Co^{III}/Co^{II}LH** couple, thus with a ~250 mV shift compared to the original Co^{III}/Co^{II} couple. Recording the cyclic voltammograms at a significantly higher scan rate (10 V s^{-1}) did not allow approaching the pure kinetic KP zone although a slightly more progressive evolution of the cathodic peak potential was observed with an increase of ~200 mV per decade of acid concentration (Table S2‡). Simulations using the DigiElch software allowed to reproduce the potential shift of such an EC process at both 0.1 and 10 mV s^{-1} using a protonation equilibrium constant higher than 10^4 and a bimolecular protonation rate of 10^7 mol^{-1} L s^{-1}, suggesting that the amine moiety can potentially act as a proton relay during catalysis.[32]

Protonation of the Co^{II} state should also alter the standard potential of the Co^{II}/Co^{I} couple. At 100 mV s^{-1}, this redox process is hidden by the catalytic wave it triggers. However, measuring cyclic voltammograms at 10 V s^{-1} enabled the catalysis to be outrun and a reversible wave to be recovered centred at −0.89 V *vs.* Fc^+/Fc (Fig. 2 bottom) that likely corresponds to the actual **Co^{II}LH/Co^{I}LH** couple responsible for catalysis. Remarkably, raising acid concentration, we found that catalysis proceeds under pure kinetic conditions, where a catalytic current plateau, independent of the scan rate, is observed (Fig. 4) because substrate consumption is negligible (pure kinetic KS zone).[31,33] Under these conditions, the mid-wave potential of the catalytic process is found at −0.87 V *vs.* Fc^+/Fc. Varying the catalyst concentration for a given acid concentration showed a linear dependence of the catalytic current with the catalyst concentration (Fig. S6‡). The catalytic plateau current also linearly varies with the acid concentration (Fig. S7‡).

Together these data are consistent with a mechanism for H_2 evolution catalyzed by **Cat1** following an ECEC reaction scheme (Scheme 1), where E and C stand for electrochemical steps and chemical (*i.e.* protonation) steps and with the second reduction occurring at a potential more positive to that of the first one: reduction of the protonated Co^{II} (**Co^{II}LH**) state yields **Co^{I}LH**, which is further protonated to yield the **Co^{III}HLH** species. Further reduction of this derivative then produces the Co^{II} hydride **Co^{II}HLH** species that is further protonated to evolve H_2 and regenerate the starting **Co^{II}LH** complex. Some of the

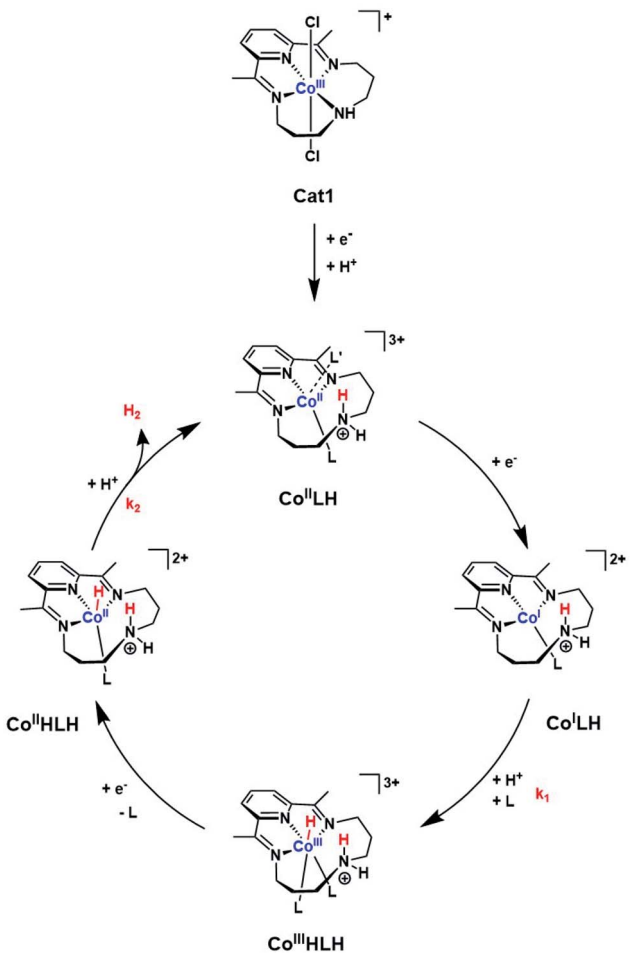

Scheme 1 Proposed ECEC mechanism for H_2 evolution mediated by **Cat1**. L and L′ indicate acetonitrile or *p*-cyanoaniline.

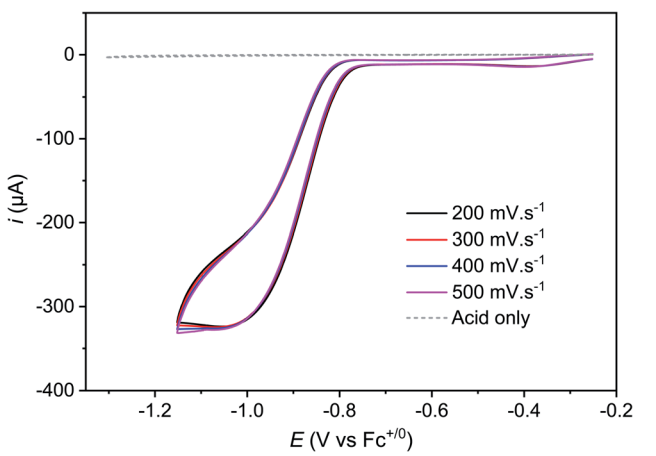

Fig. 4 Cyclic voltammograms of **Cat1** (1.6 mM) in CH_3CN (+0.1 M $^nBu_4NBF_4$) recorded at a glassy carbon electrode (1.6 mm diameter) in the presence of 60 mM *p*-cyanoanilinium tetrafluoroborate at various scan rates, scan rate ranging from 200 to 500 mV s^{-1} and with ohmic drop compensation. A control voltammogram of 60 mM *p*-cyanoanilinium tetrafluoroborate without **Cat1** at 100 mV s^{-1} is shown for comparison.

distorded geometries displayed in Scheme 1 for transient intermediates involved in the catalytic cycle are approximate and we do realize that they do not correspond to ideal geometries for coordination complexes with corresponding electronic structures. Protonation of the amine residue of the macrocyclic ligand namely generates an ammonium moiety unable to coordinate the cobalt center, though with significant steric hindrance preventing for example the adoption of a perfect square planar (or octahedral) geometry favored by the d^8 (or d^6) configuration in the **Co^{I}LH** (or **Co^{III}HLH**) species, as demonstrated for the unprotonated Co^{I} (ref. 14) or Co^{III}-hydride species,[34] respectively. Of note this family of cobalt complexes can accommodate various coordination spheres as demonstrated by the heptacoordinated systems recently reported.[35,36]

Eqn (1) gives the plateau current i_p for such a process, assuming that the two electrons required to complete catalytic turnover are transferred from the electrode to the catalyst.

$$i_{pl} = 2FSC^0_{cat}\sqrt{k_2 D_{cat} C^0_{AH}} \quad (1)$$

where F is the Faraday constant, S is the geometric electrode surface area, C^0_{cat} is the concentration of the catalyst and D_{cat} is the diffusion coefficient of the catalyst, determined to be 10^{-5} cm^2 s^{-1} from the scan-rate dependence of the peak current of the first cathodic wave and the Randles–Sevcik equation (see ESI‡).

From plateau currents measured over a range of concentrations for both catalyst and acid (Fig. S6 and S7‡), we found a value of $5.3 \pm 0.1 \times 10^3$ mol^{-1} L s^{-1} for the second order rate constant k_2. The rate constant for the first protonation step k_1 of ECEC processes is accessible from the Foot-of-the-Wave Analysis (FOWA).[37,38] This analysis requires the knowledge of the apparent standard potential of the redox couple involved, *i.e.* **Co^{II}LH/Co^{I}LH**, which could be determined to −0.89 V *vs.* Fc^+/Fc using high scan rates (Fig. 2 bottom). FOWA was performed at 3 different scan rates (100, 400 and 1000 mV s^{-1}) for two different acid concentrations (5 and 25 mM) and gave a value of $2.5 \pm 0.4 \times 10^4$ mol^{-1} L s^{-1} for the second order rate constant k_1 (Fig. S8‡). The higher value of k_1 compared to k_2 is in line with the midwave of the catalytic process being shifted positively compared to the standard potential of the **Co^{II}LH/Co^{I}LH** couple.[38] Analysis of this shift using eqn (2) for the data shown in Fig. S6 and S7‡ also leads to an average value of 2.5×10^4 mol^{-1} L s^{-1} for the second order rate constant k_1, although with a much larger error margin.

$$E_{cat/2} = E^0_{Co^{II}LH/Co^{I}LH} + \frac{RT}{2F}\ln\frac{k_1}{k_2} \quad (2)$$

The k_1 value can finally be confirmed from the analysis of cyclic voltammograms recorded at low acid concentration where the system belongs to the "total catalysis" regime (Fig. 5).[31,33] In this regime, catalysis is so fast that all the acid present in the diffusion layer is consumed during the sweep of the catalytic wave. As a consequence, the unprotonated Co(II) form of **Cat1** is regenerated after catalysis and its reduction is observed at −0.96 V *vs.* Fc^+/Fc.

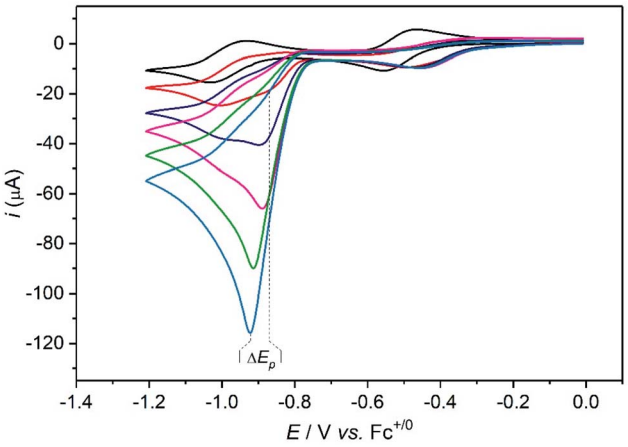

Fig. 5 Cyclic voltammograms of **Cat1** (2 mM) in CH_3CN (+0.1 M $^nBu_4NBF_4$) recorded at a glassy carbon electrode (1.6 mm diameter) in the presence of various concentrations of *p*-cyanoanilinium tetrafluoroborate at 100 mV s^{-1}: 0 (black), 4 (red), 8 (navy), 12 (magenta), 16 (green), 20 (cyan) mM.

Based on simulations, Dempsey and coworkers could propose eqn (3) to describe the variation of the catalytic peak potential E_p.[39]

$$E_p = E^0_p - 0.409\frac{RT}{F} + \frac{RT}{2F}\ln\left(\frac{RT}{F_v}\frac{D_{cat}}{D_{AH}}\frac{k_1\left(2C^0_{cat}\right)^2}{C^0_{AH}}\right) \quad (3)$$

As the intensity of the catalytic wave in the "total catalysis" regime is controlled by the diffusion of the acid, the D_{cat}/D_{AH} ratio between the diffusion coefficient of the catalyst and *p*-cyanoanilinium cation can be obtained from the ratio between the catalytic peak current and the current of the monoelectronic Co^{II}/Co^{I} wave measured in the absence of acid, according to eqn (4).

$$\frac{i_{peak}}{i^0_p} = 1.365\frac{C^0_{AH}}{C^0_{cat}}\sqrt{\frac{D_{AH}}{D_{cat}}} \quad (4)$$

Applying eqn (3) to the data shown in Fig. 5 yields a k_1 value of $2.05 \pm 0.30 \times 10^4$ mol^{-1} L s^{-1} for the second order rate constant k_1. This value is in good agreement with the one obtained by FOWA although neither k_1 nor k_2 comply with the condition of being greater than 10^7 mol^{-1} L s^{-1} required for eqn (3) to be valid.[39]

Interestingly, these data allow ruling out homolytic H_2 evolution mediated by **Cat1**. In such a mechanism, the first protonation step generating the Co^{III}–H derivative with the k_1 rate constant still exists but it is followed by reductive elimination of H_2 from two Co^{III}–H species with a k_d second-order rate constant. The linear dependency of the plateau current with the catalyst concentration (Fig. S6‡) rules out homolytic H_2 evolution from this Co^{III}–H derivative in the non-steady state where the rate-determining step is the reductive elimination step.[38,40] The identification of two distinct rate constants with k_1 being the largest one also allows to rule out steady state

homolytic H_2 evolution with the rate-determining step being the formation of the Co^{III}–H derivative, therefore implying that $k_1 < k_d$. Finally, while the mechanism proposed in Scheme 1 does not formally exclude that formation of the **Co^{III}HLH** species may proceed through intramolecular protonation of the Co^{I} center of **Co^{I}LH** followed by reprotonation of the ligand, we believe that such a possibility is unlikely as Et_3NH^+, an acid with a pK_a similar to that of the protonated $N_4H_2^+$ ligand in **Co^{I}LH**, is unable to protonate Co^{I} complexes with similar $E^0_{Co^{II}/Co^{I}}$ value such as $[Co^{I}(dmgBF_2)_2(CH_3CN)]$ ($dmgH_2$ = dimethylglyoxime) in CH_3CN.[41]

The mechanism proposed here for H_2 evolution differs from the one proposed by Llobet and Gimbert-Suriñach for aqueous conditions.[13,14] First we clearly evidenced that the Co^{II} form of **Cat1** is protonated under the conditions investigated here. Ligand protonation also occurs in aqueous electrolyte, as shown by a 59 mV pH unit $^{-1}$ shift of the redox process reported by Peters and coworkers.[19] Second, we propose that H_2 is formed from a Co^{II}–H and not a Co^{III}–H intermediate. We recognize that the electrochemical responses of ECEC and ECCE sequences, both starting from a Co^{II} derivative and implying Co^{II}–H and Co^{III}–H active species, respectively, are similar. However DFT calculations clearly demonstrated that the standard potential of the Co^{III}–H/Co^{II}–H is more positive than that of the Co^{II}/Co^{I} couple,[13] a feature also observed for cobaloximes and cobalt diimine–dioxime complexes for which the ECEC mechanism is now accepted. Importantly, the mechanism shown in Scheme 1 involves the Co^{II}HLH species that was proposed by Llobet and Gimbert-Suriñach under photocatalytic conditions,[13] therefore unifying the mechanistic understanding of this catalyst. DFT calculations previously indicated a near-thermoneutral intramolecular H_2 evolution step from this protonated hydride intermediate.[13] Our analysis shows that this step is also the rate-determining one, which explains why catalysis is so fast. Still, the observation that the rate constant of this step is first order in acid concentration suggests that intramolecular H_2 formation is coupled with protonation, either in a concerted manner or through kinetic coupling with the fast reprotonation of the amine group of the ligand.

The maximal turnover frequency (TOF_{max}) of **Cat1** therefore approximates $k_2 \times$ [acid] and a TOF_{max} value of 5.3×10^3 s^{-1} can be extrapolated for 1 M *p*-cyanoanilinium tetrafluoroborate concentration. Based on this value and an apparent equilibrium potential of the H^+/H_2 couple of −0.47 V *vs.* Fc^+/Fc at 1 M *p*-cyanoanilinium tetrafluoroborate concentration and taking homoconjugation into account,[26] we could derive the red trace in the catalytic Tafel plot[42,43] shown in Fig. 6. Interestingly, **Cat1** displays significant catalytic activity ($\log(TOF/s^{-1}) > 1$) at low overpotential values, a property shared by very few other molecular complexes including cobaloximes,[42,44] DuBois' nickel bisdiphosphine catalysts[42,45] and bis(thiosemicarbazone) cobalt[46] and nickel[47] complexes. Its overpotential requirement, estimated to be ~400 mV at the catalytic half-wave potential (and corresponding to the inflexion point in the red catalytic Tafel plot on Fig. 6) is ~100 mV higher than that of cobaloxime, cobalt diimine–dioxime[48] or DuBois' complexes. Importantly, the high TOF_{max} value also places **Cat1** in an intermediate

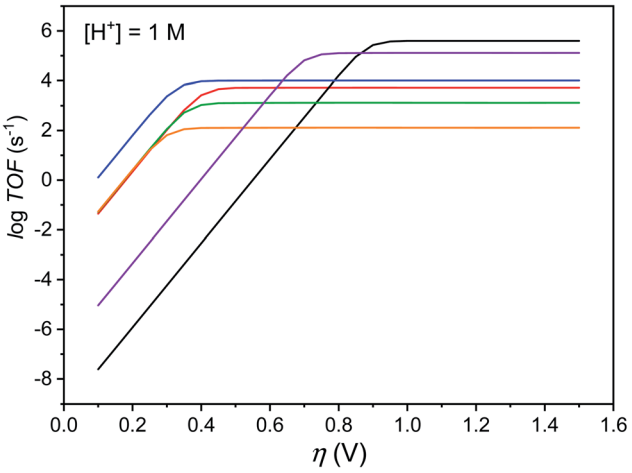

Fig. 6 Catalytic Tafel plots. Comparison of performances for H_2 evolution catalyzed by **Cat1** in CH_3CN in the presence of 1 M *p*-cyanoanilinium (red line), with other catalysts reported in the literature: black: Fe^{II}TPP, DMF, Et_3NH^+;[42,49] blue: $Co^{II}(dmgH)_2py$, DMF, Et_3NH^+;[42] green: $[Ni^{II}(P_2^{Ph}N_2^{C_6H_4X})_2]^{2+}$, X = $CH_2P(O)(OEt)_2$, MeCN, $DMFH^+$;[42,45] orange: 4-{bis[4-(*p*-methoxyphenyl)thiosemicarbazone]}-2,3-butane cobalt, DMF, Et_3NH^+;[46] purple: $[Co^{II}$(bapbpy)Cl], DMF, Et_3NH^+.[23]

position between cobaloximes and DuBois' complexes, the two champion H_2-evolving molecular catalyst series identified so far in non-aqueous solvents.[42] It is noteworthy that all three catalysts possess proton relays in their second-coordination sphere and the protonation of these relays is coupled with the metal-centered reduction step that sets the potential of the catalytic wave. The same conclusion can be reached with thiosemicarbazone nickel and cobalt complexes, with ligand-centered reduction occurring in these cases at quite positive potentials.[46,47]

Conclusions

While **Cat1** is becoming more and more popular as a molecular H_2-evolving catalyst for the design of aqueous systems, it is increasingly important to advance the understanding of its H_2 evolution catalysis mechanism[13] and performance by providing insight into the catalytic steps involved. This is especially the case when considering structural modification[50] or molecular engineering[51] in order to either enhance catalytic activity or stability[16] or immobilise a catalytic centre for integration in photoelectrodes[7–9] or devices. In the societal context, both of these objectives are ultimately necessary to achieve industrial relevancy and technological maturity of hydrogen-producing electrolysers based on molecular catalysts made from earth-abundant elements.[2,4]

In this study, new EPR evidence for the structure of the Co^{II} state of the catalyst and its dependence on the presence and nature of the acid has been presented, as well as NMR and cyclic voltammetry data indicating that fast protonation of the ligand occurs at the Co^{II} stage. Carrying on from previous work in the literature,[13,14,22] these results reconcile mechanisms at play under electrochemical and photochemical conditions.

Furthermore, a proper utilisation of the most advanced analytical methods available for molecular catalysis of electrochemical reactions has allowed definitively ruling out a homolytic H_2 evolution mechanism and substantiated the proposed heterolytic ECEC mechanism, for which the rate constants for the two successive protonation steps could be determined. The rate-determining step has been confirmed as the intramolecular H_2 evolution step, surmised to be coupled to the second protonation, thereby regenerating a protonated ligand and thus acting as a proton relay in catalysis,[32] which, interestingly, is at variance with the behaviour of the dioxime bridge in cobalt diimine–dioxime complexes.[48] Catalytic Tafel plots could be derived to enable the benchmarking of the H_2 evolution performance of **Cat1** alongside other highly efficient catalysts and confirm its place on the podium.

Conflicts of interest

There are no conflicts to declare.

Acknowledgements

This work received funding from the French National Research Agency (Labex ARCANE, CBH-EUR-GS, ANR-17-EURE-0003), the European Research Council and European Commission's Seventh Framework Program (FP7/2007–2013) under grant agreement no. 306398 (project PhotocatH$_2$ode), the European Union's Horizon 2020 Research and Innovation program under grant agreement no. 765376 (eSCALED Marie Curie ITN project). C-B. L. acknowledges support from the Chinese Scientific Council for a post-doctoral scholarship.

References

1 V. Artero, M. Chavarot-Kerlidou and M. Fontecave, *Angew. Chem., Int. Ed.*, 2011, **50**, 7238–7266.
2 J. R. McKone, S. C. Marinescu, B. S. Brunschwig, J. R. Winkler and H. B. Gray, *Chem. Sci.*, 2014, **5**, 865–878.
3 N. Queyriaux, R. T. Jane, J. Massin, V. Artero and M. Chavarot-Kerlidou, *Coord. Chem. Rev.*, 2015, **304–305**, 3–19.
4 L. Tong, L. Duan, A. Zhou and R. P. Thummel, *Coord. Chem. Rev.*, 2020, **402**, 213079.
5 V. S. Thoi, Y. J. Sun, J. R. Long and C. J. Chang, *Chem. Soc. Rev.*, 2013, **42**, 2388–2400.
6 J. L. Karn and D. H. Busch, *Nature*, 1966, **211**, 160–162.
7 S. Bold, J. Massin, E. Giannoudis, M. Koepf, V. Artero, B. Dietzek and M. Chavarot-Kerlidou, *ACS Catal.*, 2021, **11**, 3662–3678.
8 C. Nie, W. Ni, L. Gong, J. Jiang, J. Wang and M. Wang, *J. Mater. Chem. A*, 2019, **7**, 27432–27440.
9 C. Nie, C. Liu, L. Gong and M. Wang, *J. Mater. Chem. A*, 2021, **9**, 234–238.
10 R. Gueret, C. E. Castillo, M. Rebarz, F. Thomas, A. A. Hargrove, J. Pecaut, M. Sliwa, J. Fortage and M. N. Collomb, *J. Photochem. Photobiol., B*, 2015, **152**, 82–94.
11 S. Varma, C. E. Castillo, T. Stoll, J. Fortage, A. G. Blackman, F. Molton, A. Deronzier and M. N. Collomb, *Phys. Chem. Chem. Phys.*, 2013, **15**, 17544–17552.
12 C. Gimbert-Surinach, J. Albero, T. Stoll, J. Fortage, M. N. Collomb, A. Deronzier, E. Palomares and A. Llobet, *J. Am. Chem. Soc.*, 2014, **136**, 7655–7661.
13 S. Grau, M. Schilling, D. Moonshiram, J. Benet-Buchholz, S. Luber, A. Llobet and C. Gimbert-Suriñach, *ChemSusChem*, 2020, **13**, 2745–2752.
14 D. Moonshiram, C. Gimbert-Suriñach, A. Guda, A. Picon, C. S. Lehmann, X. Zhang, G. Doumy, A. M. March, J. Benet-Buchholz, A. Soldatov, A. Llobet and S. H. Southworth, *J. Am. Chem. Soc.*, 2016, **138**, 10586–10596.
15 C. H. Lee, D. Villagran, T. R. Cook, J. C. Peters and D. G. Nocera, *ChemSusChem*, 2013, **6**, 1541–1544.
16 M. Sandroni, R. Gueret, K. D. Wegner, P. Reiss, J. Fortage, D. Aldakov and M. N. Collomb, *Energy Environ. Sci.*, 2018, **11**, 1752–1761.
17 R. Gueret, L. Poulard, M. Oshinowo, J. Chauvin, M. Dahmane, G. Dupeyre, P. P. Laine, J. Fortage and M. N. Collomb, *ACS Catal.*, 2018, **8**, 3792–3802.
18 S. Roy, M. Bacchi, G. Berggren and V. Artero, *ChemSusChem*, 2015, **8**, 3632–3638.
19 C. C. L. McCrory, C. Uyeda and J. C. Peters, *J. Am. Chem. Soc.*, 2012, **134**, 3164–3170.
20 N. Kaeffer, A. Morozan, J. Fize, E. Martinez, L. Guetaz and V. Artero, *ACS Catal.*, 2016, **6**, 3727–3737.
21 V. Artero and M. Fontecave, *Chem. Soc. Rev.*, 2013, **42**, 2338–2356.
22 C. F. Leung, Y. Z. Chen, H. Q. Yu, S. M. Yiu, C. C. Ko and T. C. Lau, *Int. J. Hydrogen Energy*, 2011, **36**, 11640–11645.
23 N. Queyriaux, D. Y. Sun, J. Fize, J. Pecaut, M. J. Field, M. Chavarot-Kerlidou and V. Artero, *J. Am. Chem. Soc.*, 2020, **142**, 274–282.
24 C. Römelt, T. Weyhermüller and K. Wieghardt, *Coord. Chem. Rev.*, 2019, **380**, 287–317.
25 A. M. Appel, S. J. Lee, J. A. Franz, D. L. DuBois, M. R. DuBois and B. Twamley, *Organometallics*, 2009, **28**, 749–754.
26 V. Fourmond, P. A. Jacques, M. Fontecave and V. Artero, *Inorg. Chem.*, 2010, **49**, 10338–10347.
27 J. Niklas, K. L. Mardis, R. R. Rakhimov, K. L. Mulfort, D. M. Tiede and O. G. Poluektov, *J. Phys. Chem. B*, 2012, **116**, 2943–2957.
28 T. Arcos, B. de Castro, M. J. Ferreira, M. Rangel and J. B. Raynor, *J. Chem. Soc., Dalton Trans.*, 1994, 369–377.
29 A. Bakac and J. H. Espenson, *J. Am. Chem. Soc.*, 1984, **106**, 5197–5202.
30 A. Bhattacharjee, E. S. Andreiadis, M. Chavarot-Kerlidou, M. Fontecave, M. J. Field and V. Artero, *Chem.–Eur. J.*, 2013, **19**, 15166–15174.
31 J. M. Savéant, *Elements of Molecular and Biomolecular Electrochemistry*, Wiley, 2006.
32 J. M. Saveant, *Angew. Chem., Int. Ed.*, 2019, **58**, 2125–2128.
33 J. M. Saveant and K. B. Su, *J. Electroanal. Chem.*, 1984, **171**, 341–349.
34 A. F. M. M. Rahman, W. G. Jackson, A. C. Willis and A. D. Rae, *Chem. Commun.*, 2003, 2748–2749.

35 J.-W. Wang, K. Yamauchi, H.-H. Huang, J.-K. Sun, Z.-M. Luo, D.-C. Zhong, T.-B. Lu and K. Sakai, *Angew. Chem., Int. Ed.*, 2019, **58**, 10923–10927.
36 R. Gueret, C. E. Castillo, M. Rebarz, F. Thomas, M. Sliwa, J. Chauvin, B. Dautreppe, J. Pécaut, J. Fortage and M.-N. Collomb, *Inorg. Chem.*, 2019, **58**, 9043–9056.
37 C. Costentin, S. Drouet, M. Robert and J.-M. Savéant, *J. Am. Chem. Soc.*, 2012, **134**, 11235–11242.
38 C. Costentin and J.-M. Savéant, *ChemElectroChem*, 2014, **1**, 1226–1236.
39 E. S. Rountree, D. J. Martin, B. D. McCarthy and J. L. Dempsey, *ACS Catal.*, 2016, **6**, 3326–3335.
40 C. Costentin, H. Dridi and J.-M. Savéant, *J. Am. Chem. Soc.*, 2014, **136**, 13727–13734.
41 C. Baffert, V. Artero and M. Fontecave, *Inorg. Chem.*, 2007, **46**, 1817–1824.
42 V. Artero and J.-M. Saveant, *Energy Environ. Sci.*, 2014, **7**, 3808–3814.
43 C. Costentin, S. Drouet, M. Robert and J. M. Saveant, *Science*, 2012, **338**, 90–94.
44 M. Razavet, V. Artero and M. Fontecave, *Inorg. Chem.*, 2005, **44**, 4786–4795.
45 U. J. Kilgore, J. A. S. Roberts, D. H. Pool, A. M. Appel, M. P. Stewart, M. R. DuBois, W. G. Dougherty, W. S. Kassel, R. M. Bullock and D. L. DuBois, *J. Am. Chem. Soc.*, 2011, **133**, 5861–5872.
46 T. Straistari, R. Hardre, J. Fize, S. Shova, M. Giorgi, M. Reglier, V. Artero and M. Orio, *Chem.–Eur. J.*, 2018, **24**, 8779–8786.
47 T. Straistari, J. Fize, S. Shova, M. Réglier, V. Artero and M. Orio, *ChemCatChem*, 2016, 2262–2268.
48 D. Sun, A. K. Harshan, J. Pecaut, S. Hammes-Schiffer, C. Costentin and V. Artero, *Chemelectrochem*, 2021, **8**, 2671–2679.
49 I. Bhugun, D. Lexa and J. M. Saveant, *J. Am. Chem. Soc.*, 1996, **118**, 3982–3983.
50 W. X. Nie, D. E. Tarnopol and C. C. L. McCrory, *J. Am. Chem. Soc.*, 2021, **143**, 3764–3778.
51 N. Coutard, N. Kaeffer and V. Artero, *Chem. Commun.*, 2016, **52**, 13728–13748.